Xie, Boxuan; Dowhuszko, Alexis; Koskinen, Kalle; Mela, Lauri; Lietzen, Jari; Ruttik, Kalle; Jäntti, Riku; Hämäläinen, Jyri

Integration of Visible Light and Backscatter Communications for Ambient Internet of Things

Published in:
Proceedings of the 2024 IEEE 99th Vehicular Technology Conference

DOI:
10.1109/VTC2024-Spring62846.2024.10682827

Published: 01/01/2024

Document Version
Peer-reviewed accepted author manuscript, also known as Final accepted manuscript or Post-print

Please cite the original version:
Xie, B., Dowhuszko, A., Koskinen, K., Mela, L., Lietzen, J., Ruttik, K., Jäntti, R., & Hämäläinen, J. (2024). Integration of Visible Light and Backscatter Communications for Ambient Internet of Things. In *Proceedings of the 2024 IEEE 99th Vehicular Technology Conference* (IEEE Vehicular Technology Conference). IEEE. https://doi.org/10.1109/VTC2024-Spring62846.2024.10682827

Integration of Visible Light and Backscatter Communications for Ambient Internet of Things

Boxuan Xie, Alexis Dowhuszko, Kalle Koskinen, Lauri Mela, Jari Lietzén, Kalle Ruttik, Riku Jäntti, Jyri Hämäläinen
Department of Information and Communications Engineering, Aalto University, 02150 Espoo, Finland
Email: {firstname.lastname}@aalto.fi

***Abstract*—Ambient backscatter communication (AmBC) is a key enabler for green Internet of Things (IoT) employing ambient radio frequency (RF) signals for low-power communication. The AmBC devices discussed in the literature so far harvest light to power their microcontrollers for controlling RF modulation and reflection circuits. The ubiquitous presence of configurable light-emitting diodes (LEDs) based luminaires can also leverage such control functionalities by involving visible light communication (VLC). In this paper, we propose a visible light-enabled AmBC system that integrates VLC and AmBC for future ambient power-enabled IoT. We design LiBD, a backscatter device (BD) that uses visible light signals for both modulation control and energy supply. We demonstrate the real-time end-to-end data transmission with a proof of concept experiment. Evaluation results show that the LiBD supports multiple sub-6 GHz RF bands and can receive modulated light at frequencies up to 250 kHz. The investigations verify the feasibility of integrating the VLC and AmBC for future green IoT systems.**

***Index Terms*—Ambient backscatter communication, visible light communication, ambient IoT, green IoT.**

I. INTRODUCTION

Ambient backscatter communication (AmBC) has gained popularity in the ambient power-enabled Internet of Things (IoT) in the beyond 5G (B5G) landscape [1], offering a green communication technology alternative characterized by low-power data exchanges and low-complexity system implementations [2]. The AmBC technology employs ambient radio frequency (RF) signals, allowing low-power backscatter devices (BDs) and readers to communicate efficiently [3]. With energy harvesting and simple modulation features, the AmBC mitigates challenges of energy availability, interference confinement, and high device costs that are common in conventional IoT systems [4].

The BD transmits data by modulating and reflecting ambient RF signals, avoiding the use of energy-intensive and expensive radio components. This leads to a notable reduction in energy consumption and addresses environmental concerns linked to the widespread use of batteries in state-of-the-art IoT devices [5]. In the battery-free AmBC landscape, the BDs are mainly powered by harvested energy from radios [6] and light [7]–[9], marking a significant stride towards eco-friendly and energy-efficient communications. The radio energy harvesting for powering the BD is often a challenging task due to the propagation and penetration losses that RF signals experience. Therefore, harvesting energy using solar cells from the luminaries that irradiate strong electromagnetic signals in the visible light band provides more promising solutions.

In the realm of ultra-low-power AmBC, leveraging visible light as a power supply of the BD, is essential to the implementation of zero-energy devices. Most existing BDs harvest light only for supplying energy to their internal control and modulation circuitry. Phan-Huy et al. [7] elaborated on an ambient light-powered BD for continuous asset tracking via mobile networks. Vena et al. [8] introduced a solar-powered ambient backscatter node that operated at the 900 MHz mobile communication band. Daskalakis et al. [9] demonstrated a solar-powered backscatter sensor for monitoring plant water stress. However, all these AmBC implementations listed above only consider harvesting energy from light to power the conventional BD, which typically consists of a light harvester, a microcontroller unit (MCU), and a modulator, as shown in Fig. 1a. The modulation and backscattering in these cases must rely on the control functionalities of MCUs, which imply a power consumption that ranges from microwatts to milliwatts. The ubiquitous presence of configurable lighting, such as light-emitting diodes (LEDs), can also leverage such control functionalities through involving visible light communication (VLC). This area remains unexplored.

To the best of our knowledge, this paper is the *first* to simultaneously adopt the harvested light at the BD simultaneously for two proposes: i) Control the BD with modulated light signals embedded with the desired information; ii) Power the BD using the energy of light signals. Without applying the MCU, our proposed LiBD design reduces the implementation complexity and power consumption caused by the MCU operation, shown in Fig. 1b. In our proposed visible light-enabled AmBC scheme, the light harvester of LiBD first converts the received modulated light into electrical signals which control and power the modulator of LiBD. The control signal is then used to modulate the ambient RF carrier waves. The resulting backscattered signal is finally received by readers with the aid of conventional RF front-ends. This technique avoids modification to the existing IoT infrastructures, simplifies the control mechanism, and reduces device costs.

This work makes the following contributions:

- We propose a system architecture that integrates the VLC and AmBC to enable an ultra-low-power and low-complexity communication scheme. We demonstrate a system proof of concept with a real-time data transmission experiment. Because of its simplicity, the proposed system admits a great future potential in the field of ambient power-enabled IoT;

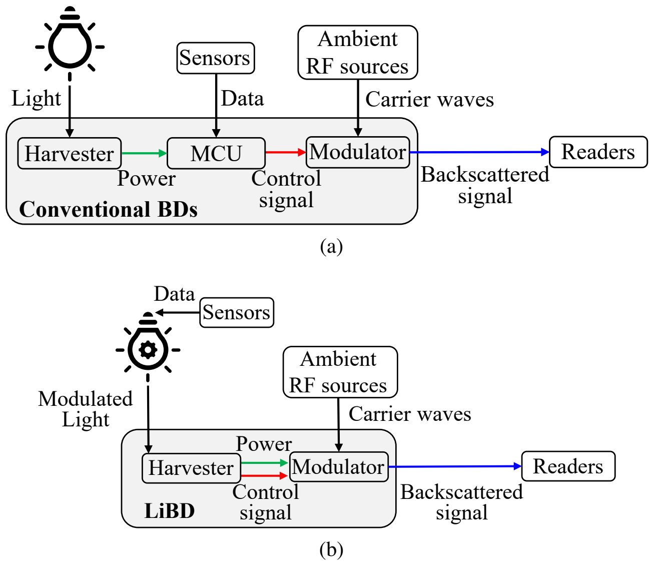

Fig. 1: Operation comparison: (a) Conventional BDs in AmBC, (b) proposed LiBD in visible light-enabled AmBC.

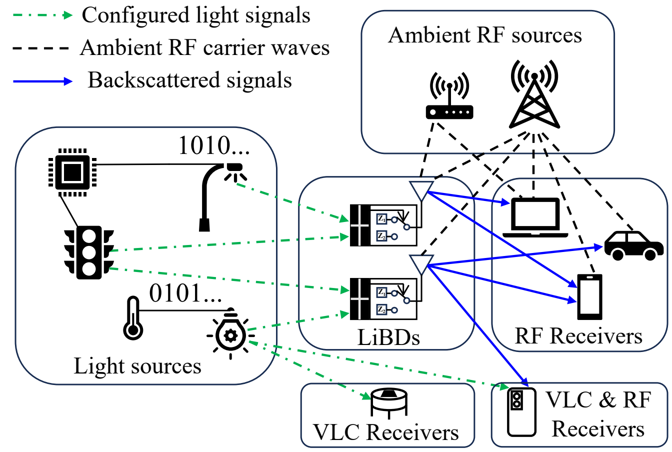

Fig. 2: System architecture of visible light-enabled AmBC.

- We design a light-controlled and -powered LiBD that serves as a bridge or relay between VLC and AmBC networks. Using two commonly used BD evaluation metrics, namely the reflection coefficient and the modulation factor [10], we show that the LiBD can support effective modulation and reflection across multiple sub-6 GHz frequency bands. We also compare the two parameters of the LiBD with conventional MCU-controlled BD, and validate that they perform at the same level;
- We characterize the photovoltaic conversion capability of the designed light harvester by its frequency response to modulated visible light. We verify that the used commercial-off-the-shelf solar cell can detect the modulated light signals at frequencies up to 250 kHz and convert them for controlling the backscatter modulation.

The rest of the paper is organized as follows. Section II proposes a visible light-enabled AmBC system architecture. Section III presents the design of the key system component LiBD. Section IV validates this design through a proof of concept experiment demonstrating real-time data transmission. The performance of LiBD regarding backscatter modulation and light harvesting is also evaluated in this section. Finally, Section V draws conclusions and discusses future work.

II. System Architecture

The proposed system architecture is shown in Fig. 2. The system consists of ambient RF sources, configurable light sources, LiBDs, receivers, and various sensors.

Ambient RF sources: The RF sources provide available carrier waves at multiple RF frequency bands used by cellular base stations, WLAN hotspots, and broadcast TVs. There is a notable amount of research done on the availability and capability of various ambient RF systems that support low-power indoor and outdoor AmBC [5].

Light sources: The presence of artificial and configurable luminaries using LEDs can support the system as an infrastructure. The configurable light sources consist of LEDs as well as LED drivers. The LED drivers collect desired messages from various sensors and generate electrical signals for LEDs that convert them into optical signals for transmission. Moreover, instead of acquiring data from sensors, a light source itself can be the information source.

Backscatter devices: A LiBD contains a light harvester and backscatter modulator. The light harvester collects and converts the configured light into electrical signals for both controlling the modulation and powering the device itself. With the control signals, the modulator modulates the ambient carrier waves by alternating its reflection coefficients. The modulated signals are then backscattered and can be captured by receivers equipped with RF front-ends. The LiBD serves as a bridge or relay between the VLC and AmBC networks.

Receivers: An RF receiver equipped with the RF front-end is able to receive and demodulate the backscattered signals from LiBDs, which carry the original sensor messages. Nevertheless, the receiver can also receive dedicated RF signals from ambient RF sources such as mobile communication signals and WLAN signals, depending on the desired communication schemes. There are also dedicated optical VLC receivers that directly convert the light signals into electrical signals from which the messages can be detected. Considering a receiver device equipped with both optical and RF front-ends, e.g., a mobile phone equipped with a suitable camera can receive data that is transmitted from light sources using light fidelity (LiFi). Here the line-of-sight (LoS) connection is typically needed. If the LoS condition is invalid, the RF front-end of device can receive data from the LiBDs. Such receiving methods provide alternatives for efficient communication through the VLC and/or RF.

III. Design and Implementation

In this section, we discuss the design and implementation of the LiBD that uses visible light for controlling and powering the backscatter modulation circuitry. The design

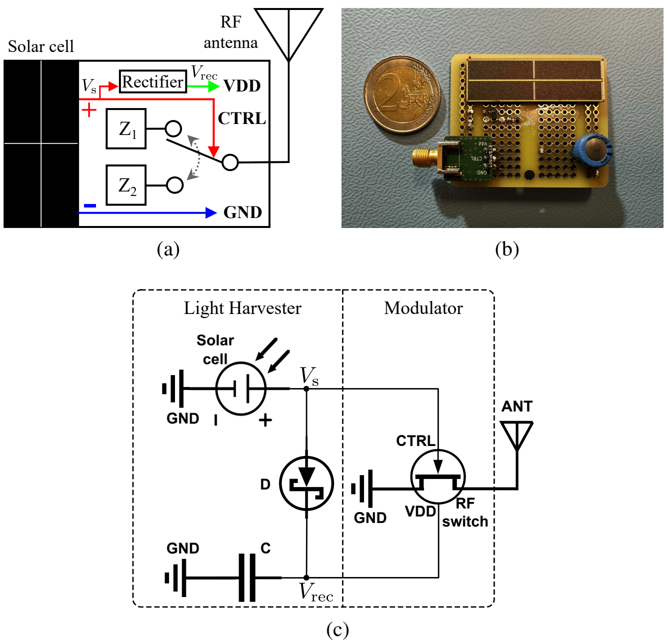

Fig. 3: LiBD design: (a) Conceptual schematic, (b) prototype (without antenna), (c) circuit diagram. A coin is placed in the picture to show the scale of the prototype.

of LiBD shown in Fig. 3 comprises the light harvester and modulator circuitry. The light harvester consists of a solar cell SM111K04L [11] as the photovoltaic converter. The solar cell harvests modulated light from configurable light sources and converts the light into the alternating current (AC) signal denoted by V_{s}. The V_{s} is sent to the control (CTRL) input of the RF switch and to the rectifier circuit, respectively. The V_{s} of the former path directly controls the switching and hence the modulation activity. The V_{s} of the latter path is first converted to the direct current (DC) signal V_{rec} by the rectifier, and then sent to the power supply (VDD) input of the switch. The rectifier in Fig. 3a employs a commonly used circuitry, including a Schottky diode 1N5819HW (D) and a 0.1 F capacitor (C) shown in Fig. 3c. In this way, the harvested light signals are efficiently utilized by the backscatter modulator, i.e., the switching component.

The backscatter modulator implementation employs an RF switch ADG919 [12] connected to the antenna, switching the termination of an antenna between two loads $Z_i \in \{Z_1, Z_2\}$. Assuming that antenna is matched to characteristic impedance Z_a, the complex reflection coefficient [10] is expressed by

$$\Gamma_i = \frac{Z_i - Z_a^*}{Z_i + Z_a}, \tag{1}$$

where * denotes the complex conjugation. The corresponding modulation factor M [10] is then

$$M = \frac{1}{4}|\Gamma_1 - \Gamma_2|^2. \tag{2}$$

The modulator achieves the maximum of $M = 1$, when $Z_1 = \infty$ and $Z_2 = 0$ corresponding to the switch either fully opening or shorting the antenna termination. The switch control signal V_{s} is converted from the modulated light signal, which originates from the baseband signal s_{b} driving the LEDs embedded with desired control information. We expect the solar cell-output signal V_{s} to keep the same waveform and phase with the LED-driving signal s_{b} for controlling the switch by the desired bit sequence. While the on-off keying (OOK) and frequency-shift keying (FSK) signals are commonly used baseband backscatter signals [13] for switching, in this work, the binary frequency shift keying (2FSK) baseband signal is implemented for data transmission such that the switching speed varies between predefined frequencies f_1 and f_2. When the ambient RF signal with a frequency of f_0 illuminates the antenna, it gets mixed with the switch control signal V_{s} by the switching operation. The modulated backscatter signals with frequencies $f_0 \pm f_1$ and $f_0 \pm f_2$ will reflect and deliver the data to the reader. The reader then detects and demodulates the backscattered signal to recover their carried information.

In the implementation, we mainly focus on demonstrating the integration of VLC and AmBC, where the LiBD serves as a significant bridge between them. Apart from the LiBD, the configurable light sources and the RF reader are key components that we will only mention briefly. The configurable lights typically consist of LEDs (or LED array) and a driver which drives LEDs with the desired baseband waveform embedded with information bits. Investigation in [14] lists the available and mature solutions. Moreover, designs of the reader or backscatter receiver are also available in our related research [15]–[17].

IV. Experiments and Evaluation

To validate and evaluate the proposed visible light-enabled AmBC system, we implement three experiments that characterize the employed device from multiple aspects. As noted before, we are mainly contributing to the BD side that integrates the VLC and AmBC efficiently. We first validate that the LED-controlled LiBD supports effective modulation and reflection over multiple RF bands by the reflection coefficient measurement and modulation factor calculation. Then, we demonstrate the system proof of concept with real-time end-to-end data transmission using a commercial-off-the-shelf light source and RF receiving instruments. Furthermore, we characterize the photovoltaic conversion capability of the light harvester (solar cell) by investigating its frequency response to the modulated light.

A. Reflection coefficient and modulation factor

The reflection coefficients of the modulator on LiBD are measured with a Rohde & Schwarz (R&S) vector network analyzer (VNA) ZNB 8 up to 4 GHz, visualized in Fig. 4 with the magnitude plot. The numerical results are shown in Tab. I, where three commonly used industrial, scientific and medical (ISM) bands and 3.5 GHz new radio (NR) band are addressed.

When LEDs are turned on and controlled by the DC, the light signal is harvested by the solar cell and converted into the

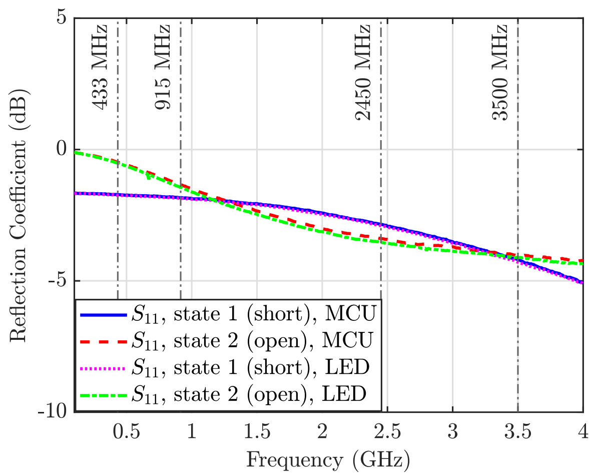

Fig. 4: VNA S_{11} measurements of the modulator controlled by the LED module and MCU.

TABLE I: VNA MEASUREMENT RESULTS.

Freq.	S_{11} SC; OC (MCU) [dB]	M (MCU)	S_{11} SC; OC (LED) [dB]	M (LED)
430 MHz	$-1.71; -0.48$	0.775	$-1.74; -0.51$	0.769
910 MHz	$-1.83; -1.33$	0.680	$-1.84; -1.43$	0.670
2450 MHz	$-2.85; -3.38$	0.480	$-3.53; -2.99$	0.469
3500 MHz	$-4.18; -4.03$	0.387	$-4.11; -4.29$	0.379

voltaic switch control signal and opens the port terminal. Once LEDs are turned off, less light is harvested and converted to the voltaic signal, and thus the switch shorts the port terminal. With this method, the RF switch either opens or shorts the measurement port terminal, contributing to two reflection coefficients Γ_1 and Γ_2, theoretically resulting in a π-phase shift from one state to the other. Applying the measured reflection coefficients, the modulation factor can be then calculated using Eq. (2). To compare the performance of the modulator under our proposed light-control technique and conventional MCU-control technique, reflection coefficients are also measured when the same modulator is directly controlled by the high (1) and low (0) level output from an MCU STM32L562 [18]. The switch either opens (OC) the port terminal with the high-level output, or shorts (SC) it with the low-level output. The comparison results are shown in Fig. 4 graphically and in Tab. I numerically, indicating the LED-controlled modulator reaches the same performance as the MCU-controlled one. Such results indicate that the LiBD is capable of modulating and reflecting the incident ambient RF signals.

B. Real-time end-to-end data transmission

In order to verify the proposed system functionality that integrates the VLC and AmBC, real-time end-to-end data transmission is demonstrated using the proof of concept setup shown in Fig. 5. The setup contains four fundamental blocks of the proposed system: the configurable light source, the ambient RF source, the backscatter device, and the reader. To avoid interference from the environment, the setup employs

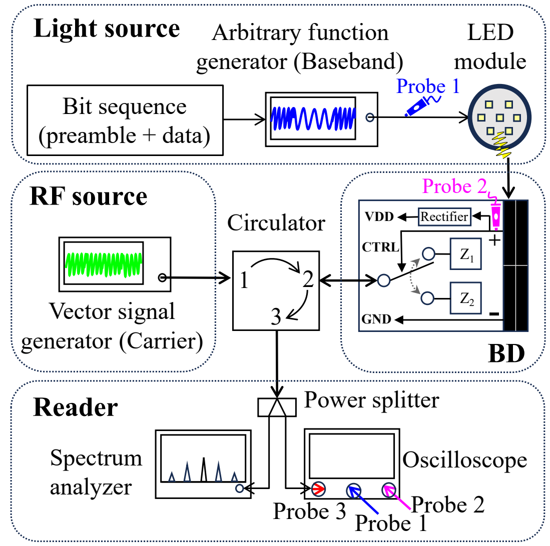

(a)

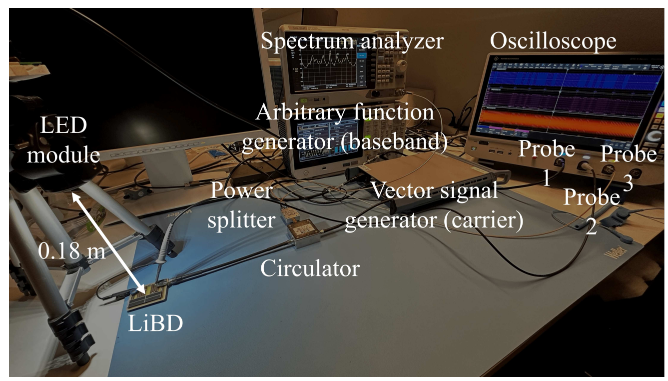

(b)

Fig. 5: Data transmission experimental setup: (a) Schematic, (b) a proof of concept setup.

a circulator for directing the RF signals between blocks with cabling instead of an over-the-air setup.

In the light source block, an arbitrary function generator sends the voltage waveform embedded with a predefined bit sequence using the 2FSK baseband modulation towards the LED driver. The predefined bit sequence consists of a 7-bit inverse Barker code preamble ’0001101’ and a 10-bit data packet ’0101110010’. The baseband signal adopts the frequency $f_1 = 250$ Hz to represent bit ’0’ whereas $f_2 = 625$ Hz represents bit ’1’. The LED driver then adapts the voltage waveform to the input current of an LED array of 7 LXML-PWC1-0100 general-purpose white LEDs [19]. The LED module then emits the configured light signal. A vector signal generator R&S SGT100A generates the continuous single-tone carrier wave at 433 MHz with an output power of -30 dBm, performing as the ambient RF source. At the LiBD, the RF switch modulates the incident carrier wave directed by a circulator with the control signal converted from the light signal harvested by the solar cell. The LiBD then reflects the modulated RF signal. A two-way power splitter

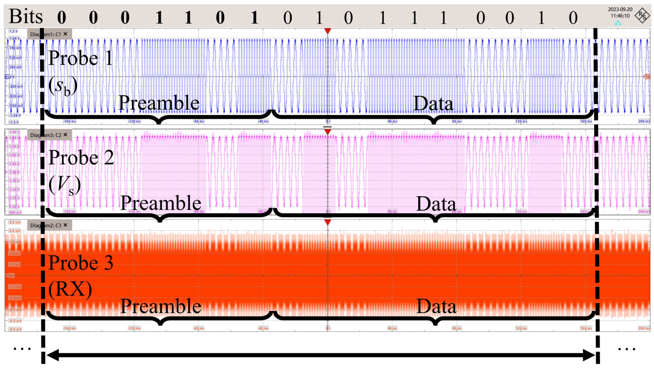

Fig. 6: Backscatter communication (data transmission) test. Probe 1 monitors the LED-control baseband signal s_{b}. Probe 2 monitors the solar cell-converted signal V_{s}. Probe 3 acquires the backscattered RF signal.

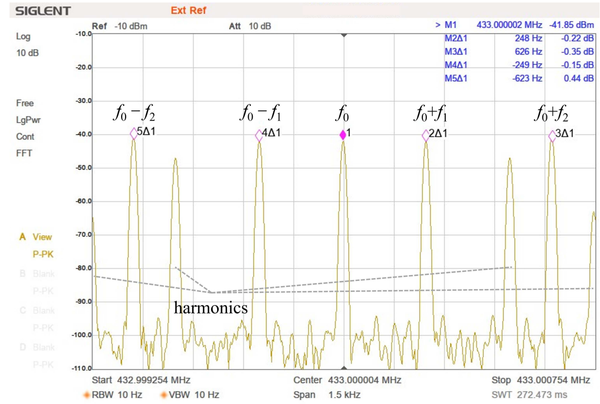

Fig. 7: Spectrum of the received signals including ambient RF carrier and backscattered signals with harmonics. The trace is maximum-held for visualizing sub-carrier components in one figure.

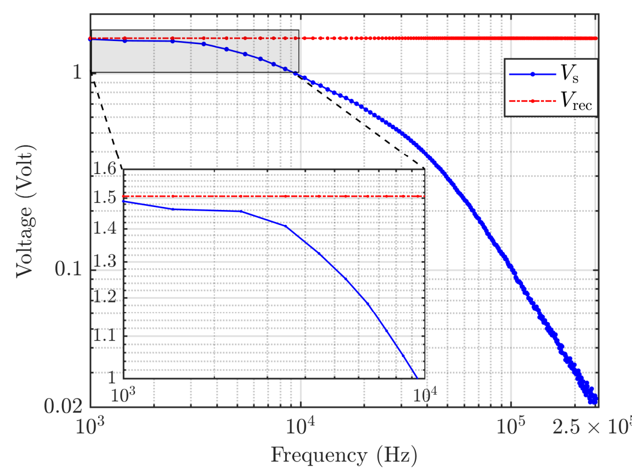

Fig. 8: Frequency characteristics of the light harvester.

splits the received signals from Port 3 of the circulator and directs them to an oscilloscope R&S RTO64 and a spectrum analyzer Siglent SSA3075XR for monitoring the waveform and spectrum, respectively. Moreover, the oscilloscope also monitors the LED-control baseband signal and the switch control signal using different probes for verification proposes.

The time-domain signals captured by the oscilloscope are displayed in Fig. 6. The baseband signal is captured by Probe 1 (blue) corresponding to the transmitted bit sequence. Further, the modulator switch control signal converted from the light is captured by Probe 2 (pink), where the baseband waveform is recovered. Finally, at the reader side, the backscattered RF signal is monitored by Probe 3 (red), where the transmitted sequence can be observed and recovered. It can be also noted that the signals monitored from the three probes are approximately synchronized in real-time. The backscattered RF signal is also delivered to the spectrum analyzer shown in Fig. 7 in the frequency domain. The signal trace is maximum held for visualizing the sub-carrier components around the carrier frequency f_0 at the frequencies $f_0 \pm f_1$ and $f_0 \pm f_2$, respectively. The observed harmonics are resulted from the nonlinearity of the RF switch, which can be filtered out by band-pass filtering in the reader design.

With this proof of concept demonstration, the end-to-end and real-time data communication from the commercial-off-the-shelf light source to the reader is verified through multiple monitoring probes placed into the system. The proposed system functionality that integrates the VLC and AmBC is therefore validated.

C. Light harvester characterization

The light harvester module of the LiBD takes the crucial responsibility of converting the light signals to voltaic signals for powering and controlling the RF switch for backscatter modulation. As shown in Fig. 3, the solar cell-output voltaic signals V_{s} flow into both the rectifier and switch control input. The rectifier further converts the V_{s} to V_{rec} as a power supply of the switch. Such conversion capabilities affect V_{s} and V_{rec}, and hence further impact the performance of the switch and modulation. The switching or modulation speed theoretically contributes to the data rate of backscatter communication, which is relevant to the V_{s} and further the modulated light signal. However, with increasing frequency of the modulated light, the magnitude of V_{s} decreases due to the low-pass feature of the solar cell [20]. Hence, it is necessary to investigate the light harvester frequency response to the modulated light.

In this case, at the light source, the baseband LED-control sine-wave signal is configured to sweep its frequency from 1 kHz to 250 kHz with 1 kHz steps. At the harvester, the peak-to-peak value of V_{s} is recorded by the oscilloscope, shown in Fig. 8 with logarithmic scale. When increasing the frequency from 1 kHz, the V_{s} continuously decreases from 1.49 to 0.02 V at 250 kHz. The V_{rec} remains around 1.51 V within the frequency range. It should be noted that the 10 dB SNR of the backscattered signal monitored at the spectrum analyzer is achieved with 250 kHz baseband LED-control signal. Beyond this frequency, the backscattered signals will further attenuate until becoming invisible on the spectrum. This is caused by the small amplitude of the V_s which is insufficient to drive the switch for backscatter modulation. Such solar cell-resulted limitation can be improved by implementing more advanced photodetectors, depending on the required throughput of the AmBC. Most existing AmBC system designs advocate for low data rate transmission with kHz-level bandwidth [5].

Moreover, the frequency response characteristic of the solar cell is investigated where a distance 0.18 m of the visible light link between the LED module and LiBD is applied. The light radiant intensity reached by the LiBD will decrease with the increase of the link distance, and thus results in a lower output voltage level of the solar cell as well as the backscatter modulation. Investigations of the solar cell-enabled VLC link distances have been reviewed in [21]. In a practical implementation, optimizing the positions of the LEDs and LiBDs is required to maximize the SNR of backscattered signals reached at receivers and hence minimize the bit errors.

With the experimental investigations, the current proof of concept is verified to support the integration of VLC and AmBC with low-complexity installments. Further investigations of over-the-air communication data rate and bit error rate will be conducted in future work.

V. Conclusion

This paper proposed the design of a visible light-enabled AmBC system that integrates VLC and AmBC for ultra-low-power connectivity of IoT devices. The system configuration combines VLC and AmBC networks and provides wireless access alternatives for various types of receivers. The LiBD has been designed and tested for this purpose which harvests configured light signals for both backscatter modulation control and energy supply. A real-time end-to-end data transmission has also been demonstrated through the system proof of concept experiment. Evaluations of the LiBD indicate that this innovation has the potential to support multiple sub-6 GHz RF bands and can adopt the modulated light at frequencies up to 250 kHz. Such investigations verify the feasibility of integrating VLC and AmBC for future ambient power-enabled green IoT configurations.

Acknowledgment

The authors appreciate Viktor Nässi for discussion and acknowledge the funding through Academy of Finland BESIMAL (Grant 334197) and WALLPAPER (Grant 352912).

References

[1] 3GPP, "Study on ambient power-enabled Internet of Things," 3rd Generation Partnership Project, TS 22.840, Jun. 2023, version 1.2.0.

[2] U. S. Toro, K. Wu, and V. C. M. Leung, "Backscatter wireless communications and sensing in green Internet of Things," *IEEE Trans. Green Commun. Netw.*, vol. 6, no. 1, pp. 37–55, 2022.

[3] V. Liu, A. Parks, V. Talla, S. Gollakota, D. Wetherall, and J. R. Smith, "Ambient backscatter: Wireless communication out of thin air," *ACM Comput. Commun. Rev.*, vol. 43, no. 4, pp. 39–50, 2013.

[4] R. Duan, X. Wang, H. Yiğitler, M. U. Sheikh, R. Jäntti, and Z. Han, "Ambient backscatter communications for future ultra-low-power machine type communications: Challenges, solutions, opportunities, and future research trends," *IEEE Commun. Mag.*, vol. 58, no. 2, pp. 42–47, 2020.

[5] T. Jiang, Y. Zhang, W. Ma, M. Peng, Y. Peng, M. Feng, and G. Liu, "Backscatter communication meets practical battery-free Internet of Things: A survey and outlook," *IEEE Commun. Surv. Tutor.*, vol. 25, no. 3, pp. 2021–2051, 2023.

[6] X. Tang, G. Xie, and Y. Cui, "Self-sustainable long-range backscattering communication using RF energy harvesting," *IEEE Internet Things J.*, vol. 8, no. 17, pp. 13 737–13 749, 2021.

[7] D.-T. Phan-Huy, D. Barthel, P. Ratajczak, R. Fara, M. d. Renzo, and J. de Rosny, "Ambient backscatter communications in mobile networks: Crowd-detectable zero-energy-devices," *IEEE J. Radio Freq. Identif.*, vol. 6, pp. 660–670, 2022.

[8] A. Vena, J. Podlecki, N. Samat, and B. Sorli, "A compact, self-powered ambient backscatter device operating in 900 MHz GSM band," in *IEEE 12th RFID-TA*, 2022, pp. 59–62.

[9] S. N. Daskalakis, G. Goussetis, S. D. Assimonis, M. M. Tentzeris, and A. Georgiadis, "A uW backscatter-morse-leaf sensor for low-power agricultural wireless sensor networks," *IEEE Sens. J.*, vol. 18, no. 19, pp. 7889–7898, 2018.

[10] J. D. Griffin and G. D. Durgin, "Complete link budgets for backscatter-radio and RFID systems," *IEEE Antennas Propag. Mag.*, vol. 51, no. 2, pp. 11–25, 2009.

[11] "Ixolar high efficiency solarmd," accessed: 04-10-2023. [Online]. Available: https://waf-e.dubudisk.com/anysolar.dubuplus.com/techsupport@anysolar.biz/O18Adzo/DubuDisk/www/Gen2/SM111K04L%20DATA%20SHEET%20202007.pdf

[12] "Wideband Mux/SPDT switches," accessed: 04-10-2023. [Online]. Available: https://www.analog.com/en/products/adg919.html#product-overview

[13] J. Kimionis, A. Bletsas, and J. N. Sahalos, "Increased range bistatic scatter radio," *IEEE Trans. Commun.*, vol. 62, no. 3, pp. 1091–1104, 2014.

[14] L. Teixeira, F. Loose, J. M. Alonso, C. H. Barriquello, V. Alfonso Reguera, and M. A. Dalla Costa, "A review of visible light communication LED drivers," *IEEE J. Emerg. Sel. Top. Power Electron.*, vol. 10, no. 1, pp. 919–933, 2022.

[15] J. Liao, X. Wang, K. Ruttik, R. Jäntti, and D.-T. Phan-Huy, "In-band ambient FSK backscatter communications leveraging LTE cell-specific reference signals," *IEEE J. Radio Freq. Identif.*, vol. 7, pp. 267–277, 2023.

[16] H. Yiğitler, X. Wang, and R. Jäntti, "Optimum multiantenna ambient backscatter receiver for binary-modulated tag signals," *IEEE Trans. Wirel. Commun.*, vol. 22, no. 2, pp. 808–823, 2023.

[17] X. Wang, H. Yiğitler, R. Duan, E. Y. Menta, and R. Jäntti, "Coherent multiantenna receiver for BPSK-modulated ambient backscatter tags," *IEEE Internet Things J.*, vol. 9, no. 2, pp. 1197–1211, 2022.

[18] "Microcontrollers - STM32L5x2," accessed: 04-10-2023. [Online]. Available: https://www.st.com/en/microcontrollers-microprocessors/stm32l5x2.html

[19] "LUXEON Rebel - general purpose white LED," accessed: 04-10-2023. [Online]. Available: https://lumileds.com/wp-content/uploads/files/DS64.pdf

[20] S. Das, E. Poves, J. Fakidis, A. Sparks, S. Videv, and H. Haas, "Towards energy neutral wireless communications: Photovoltaic cells to connect remote areas," *Energies*, vol. 12, no. 19, 2019.

[21] J. Bouclé, D. Ribeiro Dos Santos, and A. Julien-Vergonjanne, "Doing more with ambient light: Harvesting indoor energy and data using emerging solar cells," *Solar*, vol. 3, no. 1, pp. 161–183, 2023.